Applied Catalysis B: Environmental 329 (2023) 122549

Contents lists available at ScienceDirect

Applied Catalysis B: Environmental

journal homepage: www.elsevier.com/locate/apcatb

Oxidative carbonylation of methane to acetic acid on an Fe-modified ZSM-5 zeolite

Chen-Wei Wang [a,1], Yuan Sun [a,1], Li-Jun Wang [a,1], Wen-Hua Feng [a], Yu-Ting Miao [a], Ming-Ming Yu [a], Yu-Xuan Wang [a], Xu-Dong Gao [b], Qingqing Zhao [c], Zhiqin Ding [c], Zhaochi Feng [d], Si-Min Yu [a], Jinhui Yang [e], Yongfeng Hu [f], Jian-Feng Wu [a,*]

[a] State Key Laboratory of Applied Organic Chemistry, Key Laboratory of Advanced Catalysis of Gansu Province, Key Laboratory of Special Function Materials and Structure Design (MOE), College of Chemistry and Chemical Engineering, Lanzhou University, Lanzhou 730000, PR China
[b] CAS Key Laboratory of Chemistry of Northwestern Plant Resources and Key Laboratory for Natural Medicine of Gansu Province, Lanzhou Institute of Chemical Physics, Chinese Academy of Sciences (CAS), Lanzhou 730000, PR China
[c] PHI (China) Limited, Beijing 100081, PR China
[d] State Key Laboratory of Catalysis, Dalian Institute of Chemical Physics, Dalian National Laboratory for Clean Energy, Chinese Academy of Sciences, Dalian 116023, PR China
[e] State Key Laboratory of High-efficiency Utilization of Coal and Green Chemical Engineering, College of Chemistry and Chemical Engineering, Ningxia University, Yinchuan 750021, PR China
[f] Canadian Light Source, Saskatoon, Saskatchewan S7N 2V3, Canada

ARTICLE INFO

Keywords:
Methane oxidative carbonylation
Acetic acid
Iron
Zeolites
Reaction mechanisms

ABSTRACT

Direct catalytic conversion of methane under mild conditions is beneficial but challenging. Herein, we report a direct co-conversion of methane, carbon monoxide, and hydrogen peroxide into acetic acid, catalyzed by Fe/ZSM-5 (0.25) zeolite under mild conditions. The highest reported acetic acid space-time yield of ~12.01 mmol g_{cat}^{-1} h^{-1} with an optimal selectivity of 63.2% is achieved at 50 °C. This relatively high yield is ascribed to the mononuclear Fe^{3+} species. ^{13}C-Tracking experiments revealed that the methyl and carbonyl groups of acetic acid originate from methane and carbon monoxide, respectively. Spin-trapping experiments indicated that •OH and $•CH_3$ radicals are involved in the reaction. *In situ* Raman analysis suggested that –Fe–OCH_3 species is the possible intermediate. Overall, our method is greener, and our catalyst is more economical than those currently used in the industrial process. Therefore, we expect a pilot-scale test to determine the possibility as an industrial alternative.

1. Introduction

Methane is the main component of natural gas, shale gas, and combustible ice, with abundant reserves and low prices [1–3]. For these reasons, methane is considered as a potential alternative energy source for oil. In traditional industries, methane is indirectly converted to methanol from syngas (CO + H_2) via methane steam reforming [1]. However, this process has disadvantages, such as multiple reaction steps, large energy consumption, and massive investment requirements. To overcome these challenges, researchers currently focus on a direct conversion of methane to oxygenated chemicals, such as methanol [4–21], formic acid [22–25], and acetic acid [26–36].

Acetic acid is an important raw material widely used in medicine, food, and chemical industries [37]. The conventional synthesis of acetic acid (i.e., the Monsanto process [38]) involves using an expensive Rh-based catalyst, toxic CH_3I, and corrosive HI. Therefore, extensive efforts [26–36,39,40] are being focused on solving these issues by developing new catalytic systems. In 2013, we revealed the mechanism of a direct co-conversion of CH_4 and CO_2 into acetic acid on a Zn/H–ZSM-5 zeolite using solid-state NMR spectroscopy [28]. Significantly, Flytzani-Stephanopoulos [30] and Tao [31] groups subsequently reported the generation of acetic acid from CH_4, CO, and O_2 in water catalyzed by Rh-ZSM-5 zeolite at 150 °C, achieving up to 4.96 mmol g_{cat}^{-1} h^{-1} of acetic acid [30,31]. Additionally, acetic acid was produced from

* Corresponding author.
E-mail address: wjf@lzu.edu.cn (J.-F. Wu).
[1] These authors contributed equally to this work.

https://doi.org/10.1016/j.apcatb.2023.122549
Received 13 October 2022; Received in revised form 19 January 2023; Accepted 28 February 2023
Available online 1 March 2023

CH_4 and O_2 in water at 120–240 °C using an Au-ZSM-5 catalyst, yielding 0.020 mmol g_{cat}^{-1} h^{-1} of acetic acid [36]. Although the yield of acetic acid is somewhat low, the above system uses non-activated and easily available O_2 as a reactant. Owing to the scarcity of precious metals, we need to develop non-precious-metal-based catalysts to realize the co-conversion of CH_4 and CO to acetic acid. Recently, we reported preliminary results for the synthesis of Fe/ZSM-5 zeolites and the catalytic efficiency for the formation of acetic acid from CH_4, CO, and H_2O_2 [32]. Similarly, the Sun and Zhong group reported that Fe/ZSM-5 zeolites catalyzed the same conversion of CH_4, CO, and H_2O_2 to acetic acid [34]. In their study, Fe/ZSM-5 zeolites were synthesized using $FeCl_3$•$6H_2O$ as the Fe source via calcination at 400 °C, with an acetic acid space-time yield of 0.20 mmol g_{cat}^{-1} h^{-1} [34].

In this study, Fe/ZSM-5 zeolites were synthesized using the vacuum impregnation method. The Fe/ZSM-5 zeolites were synthesized using ferric acetylacetonate [$Fe(acac)_3$] as the Fe source via calcination at 500 °C. The Fe/ZSM-5 (0.25) zeolite, acting as a highly active, selective, and stable catalyst, can directly convert CH_4, CO, and H_2O_2 into acetic acid in the temperature range of 25–75 °C, reaching the highest acetic acid space-time yield reported to date of 12.01 mmol g_{cat}^{-1} h^{-1} at 50 °C and a high acetic acid selectivity of 63.2%. The relatively high acetic acid yield is ascribed to the mononuclear Fe^{3+} species, which is revealed by complementary techniques such as Diffuse Reflectance (DR) UV/Vis spectroscopy, X-ray photoelectron spectroscopy (XPS), time-of-flight secondary ion mass spectrometry (ToF-SIMS), solid-state NMR spectroscopy, and in situ Raman spectroscopy. ^{13}C-Tracking, spin-trapping, and in situ Raman experiments were used to understand the mechanism of the methane oxidative carbonylation reaction (MOCR). We expect that this study's findings and mechanistic understanding will pave the way toward the pilot-scale test for the MOCR.

2. Experimental section

2.1. Catalyst preparation

2.1.1. Preparation of the NH_4–ZSM-5 zeolite

As-synthesized ZSM-5 zeolite was calcined at 500 °C for 5 h with a ramping rate of 1 °C min^{-1} in flowing air (10 mL min^{-1}) to remove the organic template. After calcination, the obtained Na–ZSM-5 zeolite was mixed with 1 mol L^{-1} NH_4NO_3 solution for ion exchange (four times at 80 °C) to prepare NH_4–ZSM-5 zeolite. After ion exchange, the NH_4–ZSM-5 zeolite was dried overnight at 80 °C for further use.

2.1.2. Preparation of the H–ZSM-5 zeolite

The H–ZSM-5 zeolite was obtained by treating the NH_4–ZSM-5 zeolite in a muffle furnace at 500 °C for 5 h. The ICP-OES analysis indicates that the H–ZSM-5 zeolite contains 0.02 wt% of Fe.

2.1.3. Preparation of the Fe/ZSM-5 (0.25) zeolite

The Fe/ZSM-5 (0.25) zeolite was synthesized by the vacuum impregnation method. A similar procedure was reported elsewhere [28]. 0.016 g of iron acetylacetonate was dissolved in a beaker containing 5 mL of ethanol at room temperature. The iron acetylacetonate solution was then transferred to a flask containing 1 g of NH_4–ZSM-5 zeolite, which was evacuated 0.5 h in advance. The residual iron acetylacetonate solution in the beaker was washed with 5 mL of water twice, and the washing solution was also transferred into the flask. The mixture in the flask was kept stirring for 24 h at room temperature. The impregnated zeolite was dried in a rotary evaporator at 70 °C and treated in a muffle furnace at 500 °C for 3 h to obtain the Fe/ZSM-5 (0.25) zeolite, where 0.25 represents the mass percentage of $m_{Fe}/(m_{zeolite} + m_{Fe2O3})$.

2.2. Catalytic experiment

The reaction of methane, carbon monoxide, and hydrogen peroxide catalyzed by Fe/ZSM-5 (0.25) zeolite were carried out in a 100 mL glass-lined stainless steel Parr autoclave reactor. 30 mg of Fe/ZSM-5 (0.25) zeolite, 10 mL of 0.5 mol L^{-1} H_2O_2, and a stirring bar were loaded into the high-pressure reactor, and then the reactor was sealed. After that, 2 MPa of CH_4 was used to purge the air inside the reactor twice. The purging gas of CH_4 was vented outside through a piping line to ensure safe operation. The reactor was charged with CH_4 and CO to the desired pressure with an electronic pressure gauge and heated under the desired reaction temperature for a given time. Once the reactor was loaded into the heating jacket, the reaction was started by vigorously stirring at 1500 rpm. After the reaction, the reactor was placed in an ice-water bath, cooling for 0.5 h to reduce volatile products' loss. The gas products were collected by an airbag. The catalyst in liquid products was filtered by centrifuging. The liquid products were quantified by ^1H liquid NMR. Typically, 0.4 mL of filtrated reaction products and 0.1 mL of D_2O (with 0.02 wt% DSS) were loaded into a liquid NMR tube for measurement. The NMR measurement was conducted immediately after the reaction to prevent the oxidation of the products by residual H_2O_2. Besides, the NMR tube was covered with aluminum foil during transportation to avoid H_2O_2 decomposition and oxygenates oxidation. Note: The heating-up time to the desired temperature is significant to obtain the maximal yield of acetic acid. In winter, the heating-up time to 50 °C is about 8–9 min; in summer, the heating-up time to 50 °C is about 7–8 min.

3. Results and discussion

3.1. Characterization of the Fe/ZSM-5 zeolites

The Fe/ZSM-5 (0.25) zeolite was synthesized using vacuum impregnation (see Experimental Section in the Supplementary Material), where 0.25 represents the mass percentage of iron according to $m_{Fe}/(m_{zeolite} + m_{Fe2O3})$. The crystallinity of the Fe/ZSM-5 (0.25) zeolite was investigated using powder X-ray diffraction (XRD, Fig. S1). Fe_2O_3 peaks were not detected in the Fe/ZSM-5 (0.25) zeolite, suggesting that the Fe species is well dispersed, and the iron oxide particle size is below the XRD detection limit (i.e., ~4 nm). Highly ordered channels of the Fe/ZSM-5 (0.25) zeolite were observed in the transmission electron microscopy (TEM) image (Fig. 1**A**), which also shows a small number of iron oxide nanoparticles (with sizes ranging from 2.1 to 3.1 nm). DR UV/Vis spectroscopy was used to investigate the degree of agglomeration of Fe species in the Fe/ZSM-5 (0.25) zeolite under ambient conditions in the 200–800 nm range (Fig. 1**B**). The mononuclear tetrahedral (MT) Fe^{3+} species (224 nm), mononuclear octahedral (MO) Fe^{3+} species (267 nm), oligomeric Fe_xO_y clusters (355 nm), and large-sized Fe_2O_3 particles (543 nm) were observed in the DR UV/Vis spectrum [41,42]. When the Fe loading increases from 0.05 to 1 wt%, the number of oligomeric Fe_xO_y clusters and large-sized Fe_2O_3 particles significantly increases (Fig. S2). Other physicochemical properties [n(Si)/n(Al), measured Fe loading, and surface area] of the Fe/ZSM-5 (0.25) zeolite are summarized in Table S1.

Fe 2p XPS was used to characterize the chemical states of iron species on the Fe/ZSM-5 (0.25) zeolite (Fig. 1**C**). After deconvolution [6], the peaks at 711.3 and 724.2 eV were assigned to Fe $2p_{3/2}$ and Fe $2p_{1/2}$, respectively, suggesting that the Fe species is in a +3 oxidation state [43,44]. The peaks at 715.7 and 728.0 eV were due to the $Fe(OH)_x$, ($x = 1, 2, 3$) species [6].

No prominent satellite peak of Fe species is observed for the Fe/ZSM-5 (0.25) zeolite, indicating that the Fe species is highly dispersed on the catalyst surface [31]. The corresponding Si 2p, Al 2p, and O 1s XPS results for the Fe/ZSM-5 (0.25) and NH_4–ZSM-5 zeolites are presented in Fig. S3 and Tables S2–S4. ToF-SIMS was employed to investigate the structure of active sites and element linkages in the Fe/ZSM-5 (0.25) zeolite (Fig. 1**D**). $FeAlO^+$, $FeSiO_2^+$, and $FeAlSiO^+$ ions were detected in the ToF-SIMS positive spectra (Fig. 1**D**), suggesting the existence of Al–O–Fe and Si–O–Fe linkages in the Fe/ZSM-5 (0.25) zeolite. Similar findings that demonstrate the formation of Ga–O–Zr linkage on the

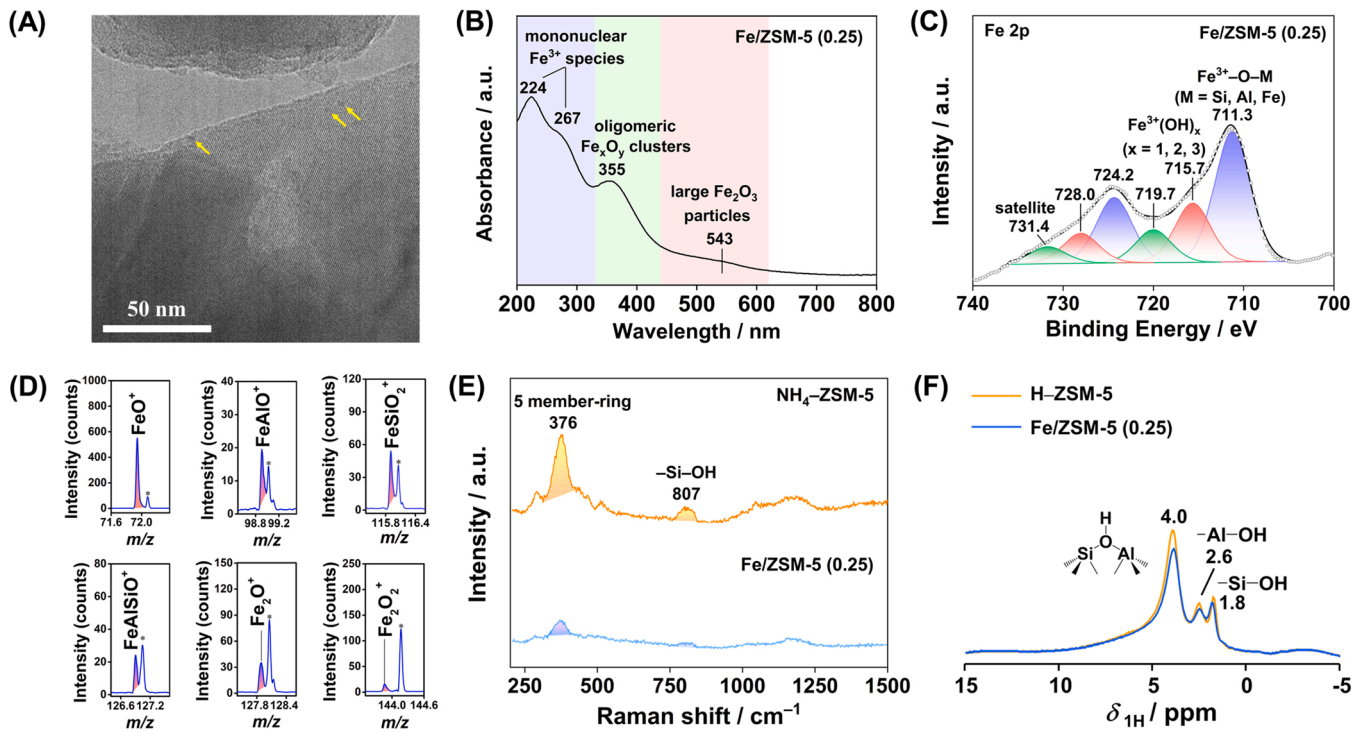

Fig. 1. Characterization of the NH_4–ZSM-5, H–ZSM-5, and Fe/ZSM-5 (0.25) zeolites. (A) TEM image of the Fe/ZSM-5 (0.25) zeolite; (B) DR UV/Vis spectrum of the Fe/ZSM-5 (0.25) zeolite; (C) Fe 2p XPS spectrum of the Fe/ZSM-5 (0.25) zeolite; (D) partial positive ToF-SIMS spectra of the Fe/ZSM-5 (0.25) zeolite; (E) UV-Raman spectra of the NH_4–ZSM-5 and Fe/ZSM-5 (0.25) zeolites; (F) solid-state ^{1}H MAS/NMR results of H–ZSM-5 and Fe/ZSM-5 (0.25) zeolites. Asterisks in (D) are attributed to two Si atoms [m ($2 \times {}^{28}$Si) = 55.9539] replacing one Fe atom [m (^{56}Fe) = 55.9349] in the labeled ions.

$GaZrO_x$ (27%) catalyst were also reported [45]. Moreover, FeO^+, Fe_2O^+, $Fe_2O_2^+$, $Fe_3O_3^+$, and $Fe_4O_4^+$ ions were observed in the Fe/ZSM-5 (0.25) zeolite, indicating that mononuclear and oligomeric Fe species were formed in the Fe/ZSM-5 (0.25) zeolite (the spectra of $Fe_3O_3^+$ and $Fe_4O_4^+$ ions with a low intensity are shown in Fig. S4). Luo and colleagues [9] reached a similar conclusion during the study of 0.1% and 0.2% Fe/ZSM-5 zeolites using ^{57}Fe Mössbauer spectroscopy. UV-Raman spectroscopy was adopted to investigate the location of Fe species in the Fe/ZSM-5 (0.25) zeolite (Fig. 1**E**). Two bands at 376 and 807 cm^{-1} decreased significantly in intensity (Fig. 1**E**) for the Fe/ZSM-5 (0.25) zeolite compared to those of the NH_4–ZSM-5 zeolite, suggesting that some Fe species is located in the 5 member-ring units of the ZSM-5 framework [46] (i.e., the band at 376 cm^{-1}) while others are bonded to the –Si–OH group [47] (i.e., the band at 807 cm^{-1}). Solid-state ^{1}H magic-angle-spinning (MAS) NMR spectroscopy was employed to investigate the changes in Brønsted acid sites after introducing Fe species into the ZSM-5 zeolite framework (Fig. 1**F**). The peak intensity of the Fe/ZSM-5 (0.25) zeolite's Brønsted acid sites (4.0 ppm) decreased significantly compared to that of the H–ZSM-5 zeolite, indicating that the Fe species replaced some of the Brønsted acid sites and were located near the bridged O in the Si–O–Al structure. This finding corresponds well with the ToF-SIMS results. Additionally, ammonia temperature-programmed desorption (NH_3-TPD) results (Fig. S5) indicate that the total acidity of the Fe/ZSM-5 (0.25) zeolite decreased with Fe introduction in comparison to that of the H–ZSM-5 zeolite. Fourier transform infrared (FTIR) spectroscopy of pyridine adsorption studies indicate that the intensity of Brønsted acid sites decreased and a new type of Lewis acid sites formed when the Fe species was introduced on the H–ZSM-5 zeolite (Fig. S6).

3.2. Acetic acid formation from methane and carbon monoxide on the Fe/ZSM-5 (0.25) zeolite at low temperatures

The effects of reaction pressure, pressure ratio of CH_4/CO, reaction temperature, reaction time, Fe loading, and H_2O_2 concentration on the catalytic performance were studied for the generation of products, as shown in Fig. 2. Each data point was obtained from at least three experiments under the same conditions.

The influence of reaction pressure on the catalytic performance is shown in Fig. 2**A**. When the pressure of CH_4 and CO increased from 1.0 + 1.0 MPa to 4.0 + 4.0 MPa, the acetic acid yield also increased. A typical ^{1}H NMR spectrum for the products obtained from the reaction of methane, carbon monoxide, and hydrogen peroxide catalyzed by the Fe/ZSM-5 (0.25) zeolite is shown in Fig. S7. Compared with other reported catalysts (Table S5), our catalyst provided the highest acetic acid yield reported to date of 6.01 mmol g_{cat}^{-1} (space-time yield = 12.01 mmol g_{cat}^{-1} h^{-1}. The corresponding conversion rates of CH_4, CO, and H_2O_2 are 19.00, 61.26, and 162.83 mmol g_{cat}^{-1} h^{-1}, respectively.) with a high acetic acid selectivity of 63.2%, with 4.0 MPa CH_4, 4.0 MPa CO, and 10 mL of 0.5 mol L^{-1} H_2O_2. Furthermore, the highest acetic acid space-time yield is ca. 2.42 times compared to the Rh-ZSM-5 zeolite [30]. The selectivity of acetic acid (Fig. 2**A**) increased with an increase in the total pressure, indicating that high reaction pressures favor the formation of acetic acid. Generally, the yields of formic acid and carbon dioxide decreased as the total pressure of CH_4 and CO increased (Fig. 2**A** and **S8A**), with both yields exhibiting a similar decreasing trend. Methanol and methyl hydrogen peroxide yields exhibited no apparent variations as the total pressure of CH_4 and CO varied (Fig. 2**A**). Through titration, we found that 57.2% of the total H_2O_2 was consumed, and at least 41.8% of the consumed H_2O_2 was involved in the MOCR with 2.5 MPa CH_4, 2.5 MPa CO, 50 °C, 0.5 h (Table S6). The corresponding calibration curves for CO_2, methanol, formic acid, and acetic acid are shown in Fig. S9 and S10.

The influence of pressure ratio of CH_4/CO on the MOCR was investigated at five different ratios: 4/1, 3/2, 2.5/2.5, 2/3, and 1/4 (Fig. 2**B**). A volcano type of acetic acid yield can be observed, and the maximum acetic acid yield was obtained at P_{CH4}/P_{CO} = 3/2. Notably, the increase in CO partial pressure from 4/1–3/2 enhanced the yield and selectivity

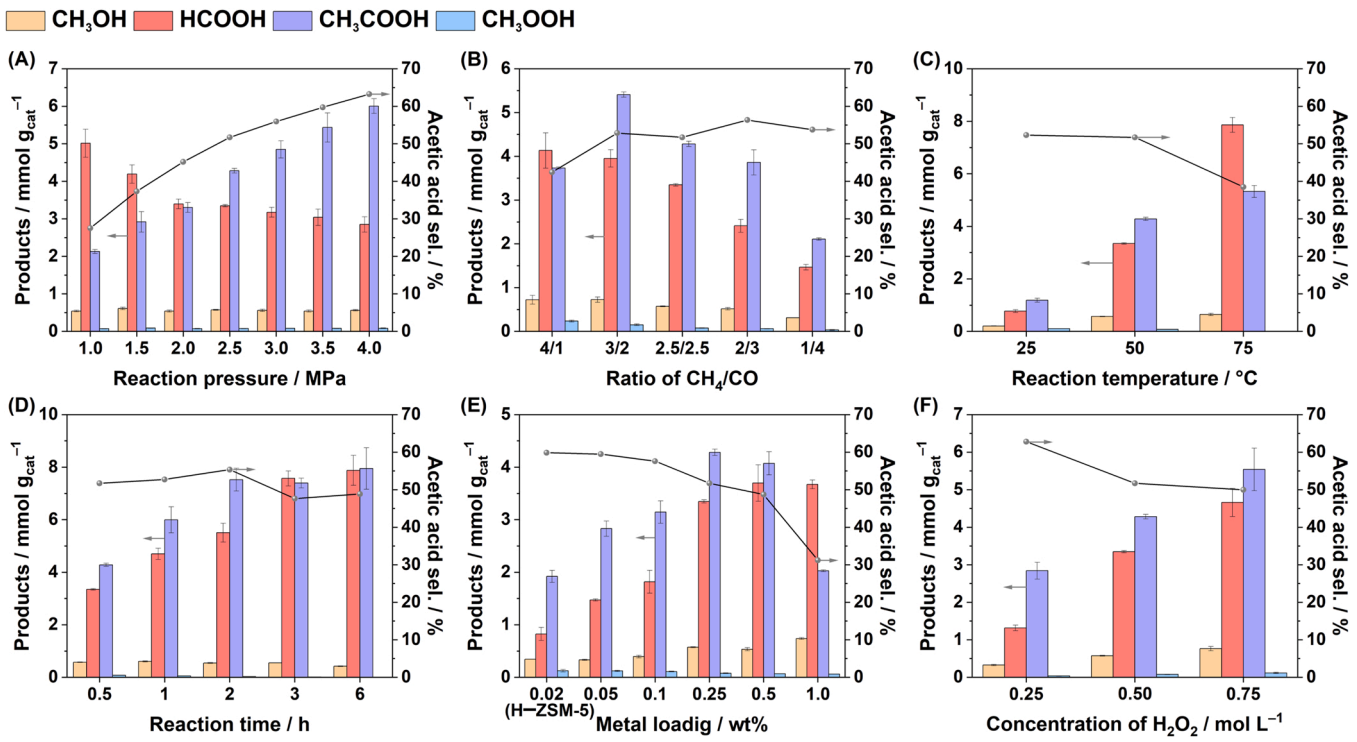

Fig. 2. Catalytic evaluation of CH_4 and CO co-reaction in the formation of acetic acid on the Fe/ZSM-5 zeolites. (A) Reaction pressure-, (B) pressure ratio of CH_4/CO-, (C) reaction temperature-, (D) reaction time-, (E) Fe loading-, and (F) H_2O_2 concentration-dependent catalytic performance during the MOCR on the Fe/ZSM-5 zeolites. Reaction conditions: 30 mg of Fe/ZSM-5 (0.25) zeolite and 10 mL of H_2O_2 were used for each reaction (E used Fe/ZSM-5 zeolites with different Fe loadings). (A) 0.5 mol L^{-1} H_2O_2, 50 °C, 0.5 h. Reaction partial pressure of CH_4 and CO are equal. For example, "2.5" means 2.5 MPa CH_4 + 2.5 MPa CO; (B) 0.5 mol L^{-1} H_2O_2, 50 °C, 0.5 h. Reaction total pressure is 5.0 MPa, for example, "2.5/2.5" means 2.5 MPa CH_4 + 2.5 MPa CO; (C) 0.5 mol L^{-1} H_2O_2, 2.5 MPa CH_4, 2.5 MPa CO, 0.5 h; (D) 0.5 mol L^{-1} H_2O_2, 2.5 MPa CH_4, 2.5 MPa CO, 50 °C; (E) 0.5 mol L^{-1} H_2O_2, 2.5 MPa CH_4, 2.5 MPa CO, 50 °C, 0.5 h; the "0.02" represent the Fe amount in the H–ZSM-5 zeolite; (F) 2.5 MPa CH_4, 2.5 MPa CO, 50 °C, 0.5 h.

of acetic acid. However, a further increase in CO partial pressure decreased the acetic acid yield. In addition, the selectivity of acetic acid maintained between 51.7% and 56.3% from P_{CH4}/P_{CO} = 3/2–1/4, suggesting that CO was in a saturated state. The decreased acetic acid yield may be due to insufficient CH_4 partial pressure. The yields of formic acid, methanol, and methyl hydrogen peroxide decreased from P_{CH4}/P_{CO} = 4/1–1/4, which may be related to the reduced CH_4 partial pressure. The sharp increase in CO_2 yield with the augment of CO partial pressure indicates that CO_2 mainly originates from the oxidation of CO (Fig. S8B).

The influence of reaction temperature on the MOCR was investigated at three different temperatures: 25, 50, and 75 °C, and the results are shown in Fig. 2**C**. Notably, the light-off temperature for the acetic acid formation is as low as 25 °C. When the reaction temperature increased from 25 to 75 °C, the acetic acid yield also increased, while the selectivity of acetic acid exhibited a similar value of ~52% at 25 and 50 °C but decreased to 38.5% at 75 °C. However, the formic acid yield increased sharply as the temperature increased from 25 to 75 °C (Fig. 2**C**). The decreased selectivity of acetic acid may be due to a dominant over-oxidation of methanol and acetic acid at 75 °C. This hypothesis is supported by the sharply increased trend of the CO_2 yield (Fig. S8C) as well as the control experiments for methanol and acetic acid oxidation by H_2O_2 (Fig. S11A and S11B). Therefore, acetic acid selectivity may be increased by suppressing over-oxidation, which can be achieved by lowering the reaction temperature. The effect of reaction temperature on the methanol yield was minor, with methanol exhibiting only a slight increase in yield as the temperature increased from 25 to 75 °C. However, the yield of methyl hydrogen peroxide decreased to zero when the reaction temperature increased to 75 °C, which may be due to its unstable nature at the higher temperature.

The influence of reaction time on the MOCR was investigated for a six-hour period (Fig. 2**D**). Acetic acid yield increased sharply from 0.5 to 2 h and increased slowly from 3 to 6 h of the reaction time. The yield of formic acid and CO_2 generally followed the same trend as that of acetic acid (Fig. 2**D** and **S8D**). This phenomenon suggests that the over-oxidation of oxygenated chemicals prevails for long reaction times (Fig. S11). Meanwhile, the yield of methanol exhibited a slightly decreasing trend over the entire six-hour period, while methyl hydrogen peroxide was not detected at reaction times beyond 3 h, which is most likely because of its instability. During the entire testing period, the selectivity of acetic acid did not change significantly, remaining between 48.0% and 55.3%.

The influence of Fe loading amounts on Fe/ZSM-5 zeolites was investigated using 0.02 (H–ZSM-5), 0.05, 0.1, 0.25, 0.5, and 1.0 wt% of Fe (Fig. 2**E**). The plot of acetic acid yield with respect to Fe loading amounts displays a volcano shape, maximizing at 0.25 wt% of Fe. However, the yield of formic acid, methanol, and CO_2 generally increased with Fe loading increased (Fig. 2**E** and **S8E**). Additionally, the selectivity of acetic acid decreased with an increase in Fe loadings. The H–ZSM-5 zeolite exhibits less activity for acetic acid formation than the Fe/ZSM-5 (0.05) catalyst (Fig. 2**E**), which due to a trace amount of Fe species (0.02 wt%, determined by the ICP-OES analysis) inside of the H–ZSM-5 zeolite. Combining this finding and the DR UV/Vis trends of the Fe species (Fig. S2), we infer that the generation of acetic acid benefits from the highly dispersed Fe species.

The influence of H_2O_2 concentration on the MOCR was investigated at three different concentrations: 0.25, 0.50, and 0.75 mol L^{-1} (Fig. 2**F**). When the H_2O_2 concentration was increased from 0.25 to 0.75 mol L^{-1}, the yields of acetic acid, formic acid, methanol, and methyl hydrogen peroxide increased. However, the selectivity of acetic acid decreased from 62.8% to 49.9%, which may be ascribed to the competing oxidizing reaction that occurs at higher concentrations of H_2O_2 (vide infra).

Although some changes are visible, the yields of CH_3COOH, HCOOH,

and CH_3OH decreased negligibly during five successive cycles for the MOCR (Fig. 3**A**), indicating that the Fe/ZSM-5 (0.25) zeolite is a stable catalyst. Similarly, the selectivity of acetic acid is also stable, ranging between 52.6% and 57.5% during the five successive cycles. The ^{27}Al MAS/NMR and XRD analyses (Fig. 3**B** and **S1**) of the used Fe/ZSM-5 (0.25) zeolite indicated no significant changes compared with those of the fresh catalyst, revealing the relative robustness of the Fe/ZSM-5 (0.25) zeolite.

3.3. Mechanistic insights into the MOCR on the Fe/ZSM-5 (0.25) zeolite

To investigate whether CO participates in acetic acid formation, we introduced CO in a control experiment. The acetic acid yield increased from 0.013 to 4.28 mmol g_{cat}^{-1}, and its corresponding selectivity increased from 0.1% to 51.7%, thereby demonstrating that CO facilitates the formation of acetic acid (Fig. 4**A** and **B**). Furthermore, the amounts of CH_3OH and HCOOH decreased along with the formation of CH_3COOH. These observations indicate that the $CH_4 \rightarrow CH_3OH \rightarrow$ HCOOH processes may be parallel competition reactions (Scheme S1). In addition, we conducted another two reactions: (1) $CH_4 + CO_2$ and (2) CH_4 + HCOOH +Ar to check the possible intermediates of CO_2 or HCOOH. However, a tiny amount of acetic acid (0.2%) was observed after reactions (Fig. 4**C** and **D**), ruling out the possible intermediates of CO_2 or HCOOH during the MOCR.

In our previous study, a trace amount of Fe ions was detected in a methane-to-methanol reaction, which likely leached out into the solution after the reaction [49]. Similarly, in this study, ICP-OES analysis revealed that 1.55% of the total Fe species leached into the solution after the MOCR (Fig. 4**A**). The leached Fe species is mainly the oligomeric Fe_xO_y clusters, which was evidenced from the DR UV/Vis analyses (Fig. S12). The Fe leaching phenomenon is mainly due to H_2O_2 and acetic acid treatment as evidenced by control experiments (not shown). To investigate whether these leached oligomeric Fe_xO_y clusters affect the reaction, we conducted the reaction with the leached Fe ions solution to determine if the reaction was homogeneous or heterogeneous. As no product was detected (Fig. 4**E**), it is plausible that the leached oligomeric Fe_xO_y clusters cannot catalyze the MOCR. Therefore, we inferred that the active sites in our catalyst are the Fe species anchored on the ZSM-5 zeolite framework. Furthermore, no acetic acid was detected without H_2O_2 (Fig. 4**F**), indicating the involvement of H_2O_2 in the MOCR (vide infra).

We then investigated the reaction mechanism to reveal the intermediates participating in the MOCR and the processes accounting for the efficient coupling of methane and CO to form the C–C bond in acetic

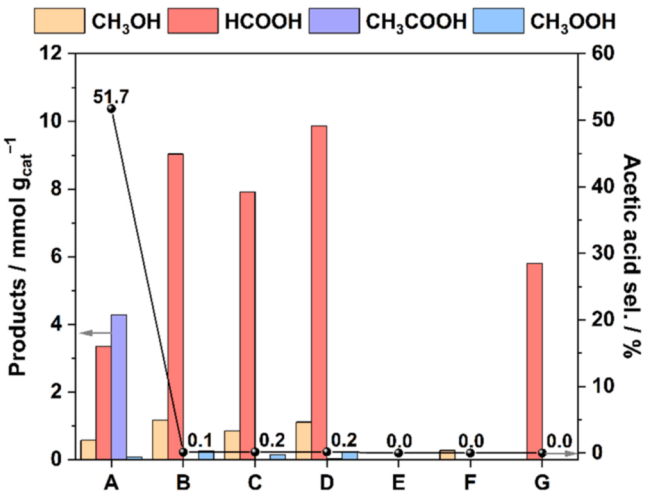

Fig. 4. Insights into the reaction of methane carbonylation on the Fe/ZSM-5 (0.25) zeolite via a comparison of catalytic results for (A) 2.5 MPa CH_4 and 2.5 MPa CO; (B) 2.5 MPa CH_4; (C) 2.5 MPa CH_4 and 2.5 MPa CO_2; (D) 2.5 MPa CH_4, 5 μL HCOOH, and 2.5 MPa Ar; (E) 2.5 MPa CH_4, 2.5 MPa CO, and leached Fe species obtained from reaction (A); (F) 2.5 MPa CH_4, 2.5 MPa CO, 10 mL of H_2O, 30 mg of the Fe/ZSM-5 (0.25) zeolite, 50 °C, and 0.5 h; (G) 2.5 MPa Ar, 5 μL CH_3OH, and 2.5 MPa CO. Reaction conditions for (A), (B), (C), (D), and (G) were: 30 mg of the Fe/ZSM-5 (0.25) zeolite, 10 mL of 0.5 mol L^{-1} H_2O_2, 50 °C, and 0.5 h. Results in part 4A were taken from Fig. 2**A** for easy comparison.

acid. Two possible reaction pathways are considered, as shown in Scheme 1. In Pathway A, methane is firstly converted into methanol, which then couples with CO to form acetic acid. The amount of methanol and formic acid (generated from the oxidation of methanol) decreased after the introduction of CO (Fig. 4**A** and **B**). Based on this observation, we hypothesized that methanol might act as an intermediate in the formation of acetic acid, similar to the Monsanto process [14,31,38,50,51]. To test whether CH_3OH carbonylation could generate acetic acid on the Fe/ZSM-5 (0.25) zeolite, CO was introduced into the reactor with methanol (Fig. 4**G**). However, no acetic acid was detected after the experiment, suggesting that "free" methanol could not be an intermediate during acetic acid formation, thereby invalidating the Pathway A hypothesis.

In Pathway B, methane and carbon monoxide were assumed to be directly coupled to produce acetic acid (Scheme 1). To probe this hypothesis, we performed a ^{13}C-tracking experiment to reveal the origin of

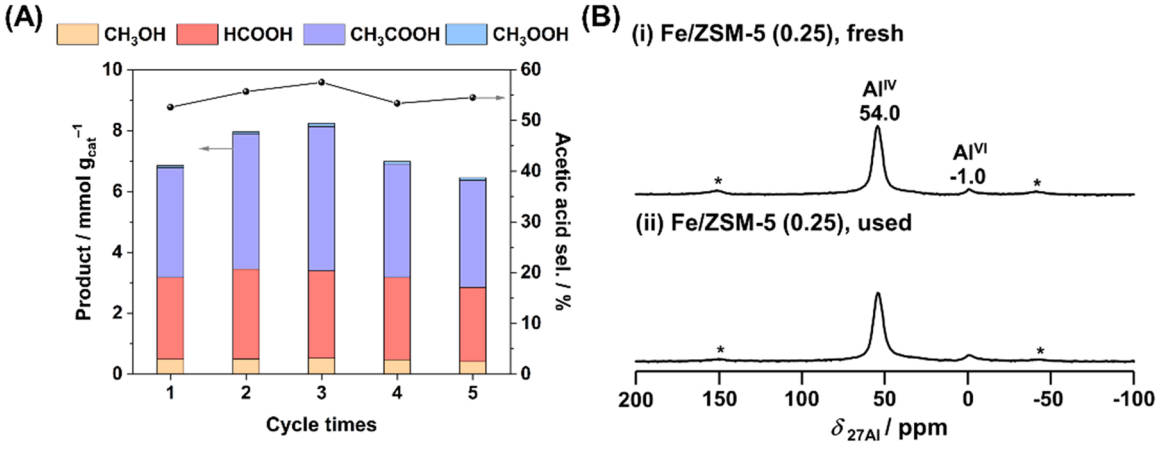

Fig. 3. (A) Product yields and acetic acid selectivity for the Fe/ZSM-5 (0.25) zeolite for five successive cycles. Reaction conditions: 30 mg of Fe/ZSM-5 (0.25) zeolite, 2.5 MPa CH_4, 2.5 MPa CO, 10 mL of 0.5 mol L^{-1} H_2O_2, 50 °C, 0.5 h. (B) ^{27}Al MAS/NMR spectra of the Fe/ZSM-5 (0.25) zeolite, (B-i) fresh Fe/ZSM-5 (0.25) zeolite, and (B-ii) used Fe/ZSM-5 (0.25) zeolite after reaction. The ^{27}Al signal at 54.0 ppm is due to 4-coordinated framework aluminum atoms (Al^{IV}), while the small signal at − 1.0 ppm is attributed to 6-coordinated aluminum atoms (Al^{VI}) [48]. The used Fe/ZSM-5 (0.25) zeolite in (B-ii) is obtained after the first cycle.

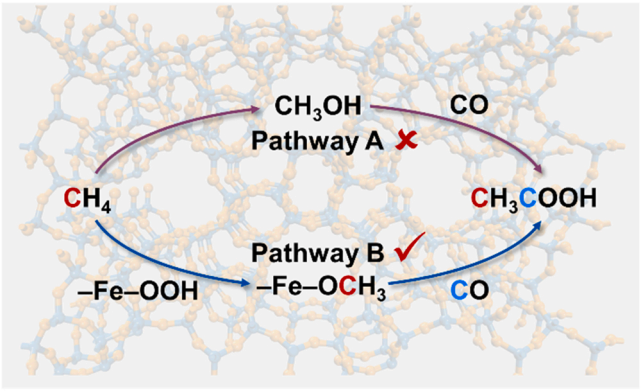

Scheme 1. Two possible reaction pathways for the formation of acetic acid from methane and carbon monoxide.

carbon atoms on the formed acetic acid (Fig. 5). A gaseous mixture of 1.0 MPa $^{13}CH_4$, 1.5 MPa CH_4, and 2.5 MPa CO was injected into the reactor with H_2O_2 and Fe/ZSM-5 (0.25) zeolite. The spectrum obtained after the reaction is displayed in Fig. 5**A**. The ^{13}C-labeled methyl group of $^{13}\underline{C}H_3COOH$ was observed at $\delta = 20.5$ ppm, while carbonyl signal was not detected, indicating that the methyl group of acetic acid originates from methane. Furthermore, $H^{13}COOH$, $HO^{13}CH_2OOH$, $HO^{13}CH_2OH$, and $^{13}CH_3OH$ were detected at $\delta = 166.8$, 92.6, 81.9, and 48.9 ppm [7,9,14], respectively, suggesting that all ^{13}C atoms in these oxygenated species are derived from methane. When the gaseous mixture composition was changed to 2.5 MPa CH_4, 1.0 MPa ^{13}CO, and 1.5 MPa CO during the MOCR (Fig. 5**B**), the ^{13}C-labeled carbonyl group of $CH_3^{13}\underline{C}OOH$ was observed at $\delta = 176.8$ ppm [10], and methyl signal was not detected, suggesting that the carbonyl group of acetic acid originates from CO. Besides, ^{13}C-labeled CO_2 was detected at $\delta = 124.5$ ppm [28], which may be due to the oxidation of ^{13}CO by H_2O_2 (Fig. S11D). Therefore, these above experiments demonstrate that the methyl group of acetic acid stems from methane and the carbonyl group from CO (Scheme 1, Pathway B).

EPR spectroscopy was used to investigate the possibility of forming a radical intermediate during the co-conversion of methane and CO

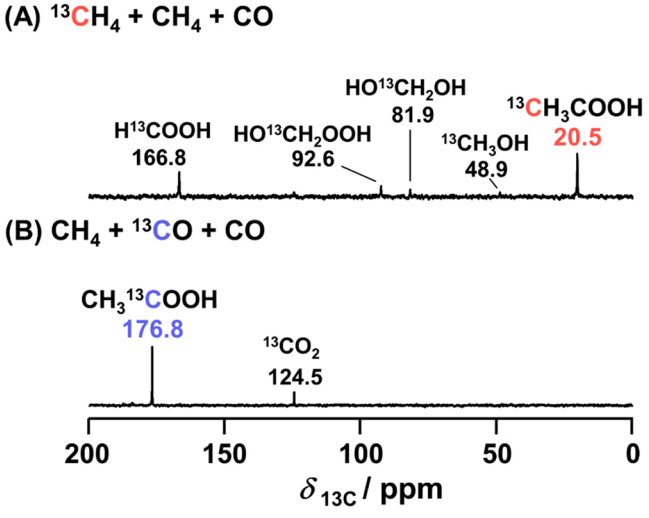

Fig. 5. Liquid NMR investigation into the origin of carbon atoms on acetic acid. ^{13}C NMR spectra were recorded upon the reaction of (A) 1.0 MPa $^{13}CH_4$, 1.5 MPa CH_4, and 2.5 MPa CO; (B) 2.5 MPa CH_4, 1.0 MPa ^{13}CO, and 1.5 MPa CO on the Fe/ZSM-5 (0.25) zeolite. Reaction conditions: 30 mg of the Fe/ZSM-5 (0.25) zeolite, 10 mL of 0.5 mol L^{-1} H_2O_2, 50 °C, 0.5 h. During these reactions, mixed ^{13}C-enriched and unlabeled methane or carbon monoxide gases were used to increase the reaction pressure.

(Fig. 6). The spin-trapping agent 5,5-dimethyl-1-pyrroline N-oxide (DMPO) was used to trap the possible free radical during the reaction. As shown in Fig. 6**A-i**, the DMPO/•OH adduct was detected with a typical four-line signal ($a^N = a^H = 14.9$ G) and $g = 2.0074$. This result is compared with the corresponding simulation result plotted as a dashed line in Fig. 6**A-ii**, which shows a nearly identical four-line signal. Furthermore, control experiments (without H_2O_2 or DMPO) produced silent signals (Fig. S13). Similar observations with DMPO/•OH adduct were reported previously for a methane oxidation reaction by our group [9] and others [14,52,53]. Additionally, methyl radical was trapped by 2,2,6,6-tetramethylpiperidine-1-oxyl (TEMPO) during the co-conversion of methane and CO (Fig. 6**B**). The methyl-TEMPO adduct was confirmed using high-resolution mass spectrometry with $[M_1 + H]^+$ and $[2\,M_1 + H]^+$ at $m/z = 172.1693$ and 343.3314, respectively. A similar strategy was successfully used by the Xu group [54]. From these results, we conclude that a free radical mechanism is involved in the MOCR.

To reveal the changes in Fe species on the Fe/ZSM-5 (0.25) zeolite during the reaction, in situ Raman spectroscopy was adopted, which is a powerful technique [55–57] that can selectively identify specific Fe species. The –Fe–OH species [58] at 745 cm^{-1} (Fig. 7**A**) decreased after Ar treatment at 450 °C (Fig. 7**B**). Further, upon the addition of H_2O_2 to the activated Fe/ZSM-5 (0.25) zeolite (Fig. 7**C**), the –Fe–OOH species [59] (632 cm^{-1}) was formed, and the –Fe–OH species (745 cm^{-1}) disappeared. When the flowing gas was switched to CH_4, the –Fe–OCH_3 species [60] and –Fe–OH species appeared at 585 and 745 cm^{-1}, respectively. In addition, the –Fe–OCH_3 species was also observed from the in situ diffuse reflectance infrared Fourier transform spectroscopy (DRIFTS, Fig. S14). The results demonstrate that the –Fe–OOH species abstracts an H-atom from methane to generate an –Fe–OCH_3 species (Scheme 1, Pathway B), a possible intermediate that further reacts with CO to form acetic acid. Similar observations with the formations of acetic acid from methoxy and CO on ZnO [48] and zinc-modified zeolites [27] further support our hypothesis. Based on the results of in situ Raman and in situ DRIFTS, an Fe species cycle is proposed in Scheme S2.

Remarkably, we found a linear correlation between the total oxygenates yield and the amount of MO Fe^{3+} species (Fig. 8**A**), after deconvoluting the DR UV/Vis spectra of Fe/ZSM-5 zeolites with Fe loadings of 0.05, 0.1, 0.25, and 0.5 wt% (Fig. S15 and Table S7). Furthermore, the acetic acid selectivity correlates with the percentage of MT Fe^{3+} species in the total Fe species (Fig. 8**B**). Therefore, we speculate that the methane activation step is directly related to the amount of MO Fe^{3+} species, and the carbonylation step correlates highly with the percentage of MT Fe^{3+} species. Similarly, the Luo group [61] found that the C1 oxygenates yield correlated with the proportion of monomeric Fe species during the methane-to-methanol reaction on the Fe/ZSM-5 zeolite. Additionally, instead of a volcano shape, the value of $TOF_{acetic\ acid}$ increased as the metal loading decreased from 1.0 wt% to 0.05 wt% (Fig. 9), which indicates the active sites are mononuclear Fe^{3+} species rather than binuclear Fe^{3+} species.

Our results demonstrate that the Fe/ZSM-5 (0.25) zeolite, acting as a highly efficient catalyst, can directly convert CH_4, CO, and H_2O_2 into acetic acid in the temperature range of 25–75 °C, with the highest acetic acid space-time yield reported to date of 12.01 mmol g_{cat}^{-1} h^{-1} and a high acetic acid selectivity of 63.2% at 50 °C. The excellent catalytic performance is ascribed to the following unique attributes of the catalytic system: (i) the Fe species anchored on zeolite (Fig. 1 and **S2**) functions as an enzyme-like catalyst [17], making the MOCR highly efficient; (ii) the acetic acid yield and selectivity decreased as the mole ratio of n(SiO_2)/n(Al_2O_3) increased, indicating that Al atoms on the ZSM-5 zeolite play an essential role in forming Fe active sites (Fig. 1 and **S16**); (iii) Fe species is highly dispersed in the Fe/ZSM-5 (0.25) zeolite (Fig. 1), thereby generating a large number of Fe mononuclear active sites (Fig. 8), which is different from the proposed mechanism of Fe binuclear active sites in the Fe-BN/ZSM-5 zeolite [34].

The precious metal catalysts (Rh- or Ru-ZSM-5) [30,31,35,40] and

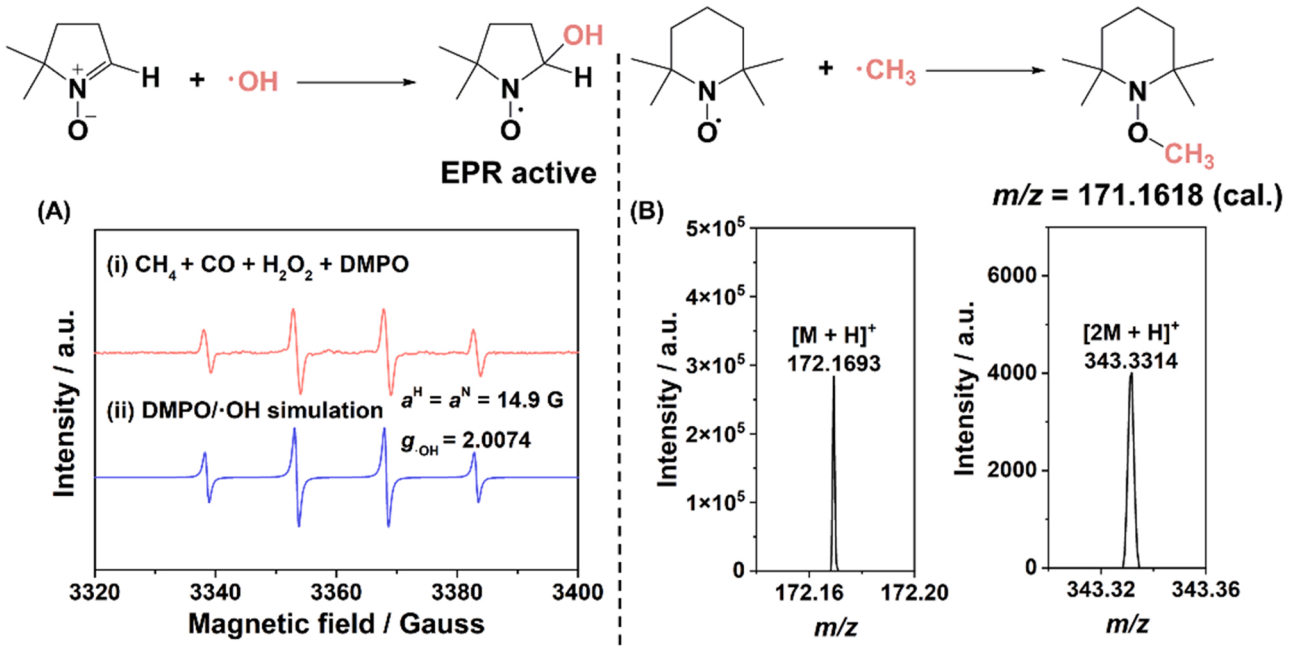

Fig. 6. Spin-trapping evidence for the radical mechanism of MOCR on the Fe/ZSM-5 (0.25) zeolite. (A-i) Small amount (~1–3 mg) of DMPO was added into the reaction system consisting of 30 mg Fe/ZSM-5 (0.25) zeolite, 2.5 MPa CH_4, 2.5 MPa CO, and 10 mL of 0.5 mol L^{-1} H_2O_2 at 50 °C after 0.5 h. (A-ii) Simulation spectrum of DMPO/•OH adduct. (B) TEMPO trapped methyl radical (•CH_3) during the reaction of 30 mg Fe/ZSM-5 (0.25) catalyst, 2.5 MPa CH_4, 2.5 MPa CO, 0.3 g TEMPO, and 10 mL of 0.5 mol L^{-1} H_2O_2 at 50 °C for 0.5 h. Methyl-TEMPO adduct was confirmed using high-resolution mass spectrometry.

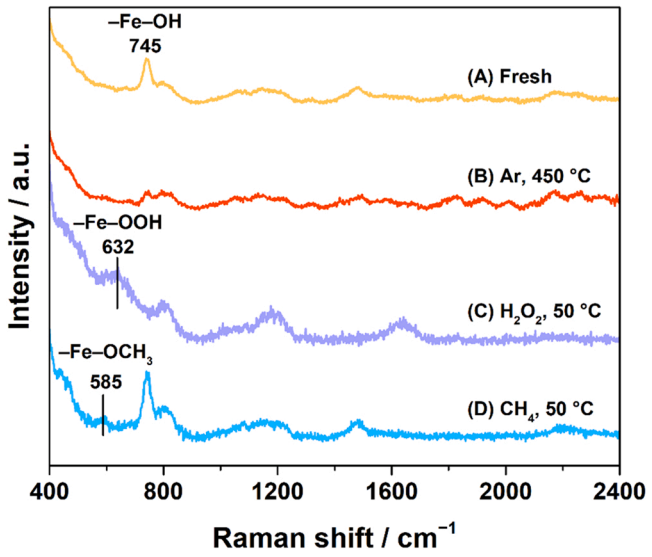

Fig. 7. In situ Raman spectra were collected for (A) the fresh Fe/ZSM-5 (0.25) zeolite; (B) the Fe/ZSM-5 (0.25) zeolite was treated with flowing Ar (20 mL min^{-1}) at 450 °C; (C) ~0.05 mL of 0.5 mol L^{-1} H_2O_2 was introduced on the surface of activated Fe/ZSM-5 (0.25) zeolite at 50 °C; and (D) CH_4/He (2%, 20 mL min^{-1}) was introduced on the Fe/ZSM-5 (0.25) zeolite at 50 °C.

the non-precious metal catalyst (Fe/ZSM-5) perform differently, but both could be alternative strategies to synthesize acetic acid from methane directly. For example, the non-precious metal catalyst can proceed at a low temperature (25–75 °C vs. 150 °C). In contrast, the precious metal catalysts can employ cheaper oxidants (O_2 vs. H_2O_2).

Compared with the Monsanto process for acetic acid synthesis (Table S8), our catalytic system has advantages in several aspects, such as low reaction temperature (25–75 °C vs. 150–200 °C), short reaction time (0.5 h vs. 17 h), easy to separate between the catalyst and products (heterogeneous catalyst vs. homogeneous catalyst), low catalyst cost (44 \$ kg^{-1} vs. 251,177 \$ kg^{-1}), and low facility cost (stainless steel 316 and glass vs. corrosion-resistant materials).

4. Conclusion

We developed an Fe/ZSM-5 (0.25) zeolite using the impregnation method and demonstrated that methane, carbon monoxide, and hydrogen peroxide can be converted into acetic acid by the highly active, selective, and stable Fe/ZSM-5 (0.25) zeolite under mild reaction conditions. The highest acetic acid space-time yield reported to date of 12.01 mmol g_{cat}^{-1} h^{-1} and a high acetic acid selectivity of 63.2% are achieved under the reaction conditions (4.0 MPa CH_4, 4.0 MPa CO, 10 mL of 0.5 mol L^{-1} H_2O_2, 50 °C, and 0.5 h). The relatively high acetic acid yield is attributed to the mononuclear Fe^{3+} species mainly located in the 5 member-ring units, where they replace some of the Brønsted acid sites. ^{13}C-Tracking experiments demonstrated that the methyl and carbonyl groups of acetic acid stem from CH_4 and CO, respectively. Spin-trapping experiments revealed that the hydroxyl and methyl radicals are involved in the MOCR. In situ Raman analysis suggested that an –Fe–OCH_3 species is the possible intermediate, generated from the reaction of methane and the –Fe–OOH species. Further, the addition of H_2O_2 on the Fe/ZSM-5 (0.25) zeolite produced the –Fe–OOH species. The current Monsanto process for the industrial production of acetic acid involves an expensive Rh catalyst, toxic CH_3I, and corrosive HI. In contrast, our catalytic method provides a new facile strategy to synthesize acetic acid by directly converting methane and carbon monoxide under mild conditions adopting the environmentally friendly hydrogen peroxide as the oxidant and the earth-abundant iron as the source of active sites. We expect to use the Fe/ZSM-5 (0.25) zeolite for a pilot-scale test as an industrial alternative to synthesizing acetic acid from CH_4 and CO.

CRediT authorship contribution statement

Chen-Wei Wang: Methodology, Validation, Formal analysis, Investigation, Visualization, Writing – original draft. **Yuan Sun:** Methodology, Validation, Formal analysis, Investigation, Visualization, Writing –

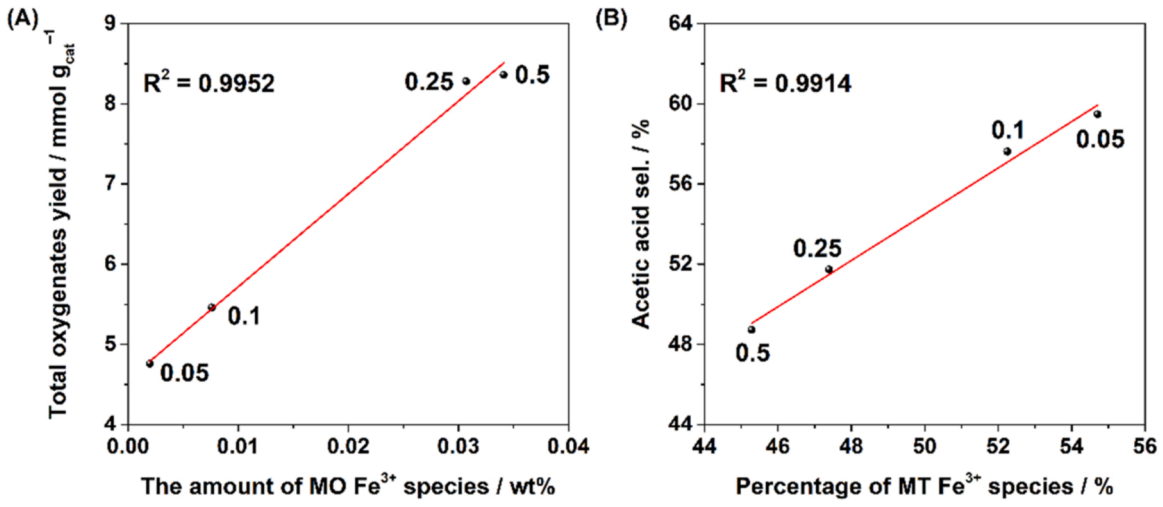

Fig. 8. (A) Linear correlation between oxygenates yield and the amount of MO Fe^{3+} species. (B) Linear correlation between acetic acid selectivity and the percentage of MT Fe^{3+} species in the total Fe species.

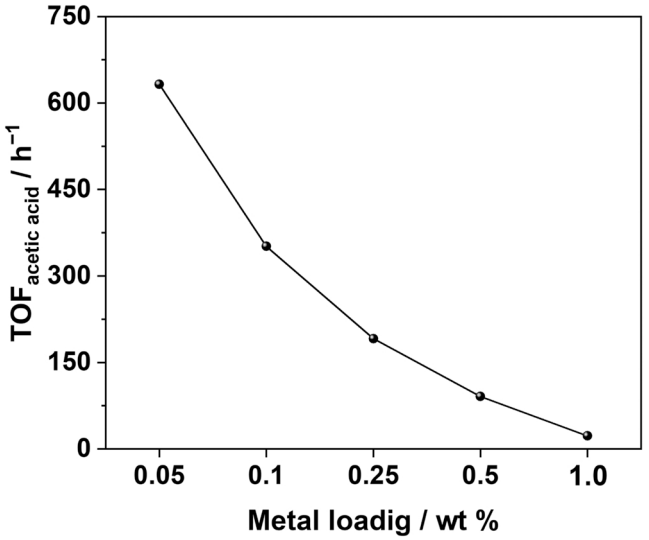

Fig. 9. Correlation between $TOF_{acetic\ acid}$ and metal loading on various Fe/ZSM-5 zeolites.

original draft. **Li-Jun Wang:** Methodology, Validation, Formal analysis, Investigation, Visualization, Writing – original draft. **Wen-Hua Feng:** Investigation, Formal analysis. **Yu-Ting Miao:** Investigation. **Ming-Ming Yu:** Investigation. **Yu-Xuan Wang:** Investigation. **Dong Gao:** Investigation. **Qingqing Zhao:** Investigation. **Zhiqin Ding:** Investigation. **Zhaochi Feng:** Resources. **Si-Min Yu:** Resources, Funding acquisition. **Jinhui Yang:** Funding acquisition. **Yongfeng Hu:** Writing – review & editing. **Jian-Feng Wu:** Conceptualization, Methodology, Investigation, Formal analysis, Visualization, Writing – review & editing, Supervision, Funding acquisition.

Declaration of Competing Interest

The authors declare that they have no known competing financial interests or personal relationships that could have appeared to influence the work reported in this paper.

Data availability

Data will be made available on request.

Acknowledgements

This project was financially supported by the National Natural Science Foundation of China (Nos. 21903041 and 21803027), Fundamental Research Funds for the Central Universities (lzujbky-2021-ey11), and Foundation of State Key Laboratory of High-efficiency Utilization of Coal and Green Chemical Engineering (Grand No. 2022-K07). We thank the Electron Microscopy Centre of Lanzhou University for the microscopy and microanalysis of our specimens. We thank Prof. Guo-Qiang Xu (Lanzhou University), Yong Cong (Lanzhou University), Wei Zhang (Ulvac-Phi), Defeng Lu (Ulvac-Phi), Yu-Fei Teng (Lanzhou University), and Cai-Ni Huang (Lanzhou University) for helpful discussion and assistance.

Appendix A. Supporting information

Supplementary data associated with this article can be found in the online version at doi:10.1016/j.apcatb.2023.122549.

References

[1] P. Schwach, X. Pan, X. Bao, Direct conversion of methane to value-added chemicals over heterogeneous catalysts: Challenges and prospects, Chem. Rev. 117 (2017) 8497–8520, https://doi.org/10.1021/acs.chemrev.6b00715.
[2] M. Ravi, M. Ranocchiari, J.A. van Bokhoven, The direct catalytic oxidation of methane to methanol—a critical assessment, Angew. Chem. Int. Ed. 56 (2017) 16464–16483, https://doi.org/10.1002/anie.201702550.
[3] X. Meng, X. Cui, N.P. Rajan, L. Yu, D. Deng, X. Bao, Direct methane conversion under mild condition by thermo-, electro-, or photocatalysis, Chem. 5 (2019) 2296–2325, https://doi.org/10.1016/j.chempr.2019.05.008.
[4] V.L. Sushkevich, D. Palagin, M. Ranocchiari, J.A. van Bokhoven, Selective anaerobic oxidation of methane enables direct synthesis of methanol, Science 356 (2017) 523–527, https://doi.org/10.1126/science.aam9035.
[5] Y. Kwon, T.Y. Kim, G. Kwon, J. Yi, H. Lee, Selective activation of methane on single-atom catalyst of rhodium dispersed on zirconia for direct conversion, J. Am. Chem. Soc. 139 (2017) 17694–17699, https://doi.org/10.1021/jacs.7b11010.
[6] J. Xie, R. Jin, A. Li, Y. Bi, Q. Ruan, Y. Deng, Y. Zhang, S. Yao, G. Sankar, D. Ma, J. Tang, Highly selective oxidation of methane to methanol at ambient conditions by titanium dioxide-supported iron species, Nat. Catal. 1 (2018) 889–896, https://doi.org/10.1038/s41929-018-0170-x.
[7] X. Cui, H. Li, Y. Wang, Y. Hu, L. Hua, H. Li, X. Han, Q. Liu, F. Yang, L. He, X. Chen, Q. Li, J. Xiao, D. Deng, X. Bao, Room-temperature methane conversion by graphene-confined single iron atoms, Chem. 4 (2018) 1902–1910, https://doi.org/10.1016/j.chempr.2018.05.006.
[8] B.E.R. Snyder, M.L. Bols, R.A. Schoonheydt, B.F. Sels, E.I. Solomon, Iron and copper active sites in zeolites and their correlation to metalloenzymes, Chem. Rev. 118 (2018) 2718–2768, https://doi.org/10.1021/acs.chemrev.7b00344.
[9] J.-F. Wu, X.-D. Gao, L.-M. Wu, W.D. Wang, S.-M. Yu, S. Bai, Mechanistic insights on the direct conversion of methane into methanol over Cu/Na–ZSM-5 zeolite: Evidence from EPR and solid-state NMR, ACS Catal. 9 (2019) 8677–8681, https://doi.org/10.1021/acscatal.9b02898.

[10] H. Zhou, T. Liu, X. Zhao, Y. Zhao, H. Lv, S. Fang, X. Wang, F. Zhou, Q. Xu, J. Xu, C. Xiong, Z. Xue, K. Wang, W.-C. Cheong, W. Xi, L. Gu, T. Yao, S. Wei, X. Hong, J. Luo, Y. Li, Y. Wu, A supported nickel catalyst stabilized by a surface digging effect for efficient methane oxidation, Angew. Chem. Int. Ed. 58 (2019) 18388–18393, https://doi.org/10.1002/anie.201912785.

[11] J. Meyet, K. Searles, M.A. Newton, M. Wörle, A.P. van Bavel, A.D. Horton, J.A. van Bokhoven, C. Copéret, Monomeric copper(ii) sites supported on alumina selectively convert methane to methanol, Angew. Chem. Int. Ed. 58 (2019) 9841–9845, https://doi.org/10.1002/anie.201903802.

[12] Z. Jin, L. Wang, E. Zuidema, K. Mondal, M. Zhang, J. Zhang, C. Wang, X. Meng, H. Yang, C. Mesters, F.-S. Xiao, Hydrophobic zeolite modification for in situ peroxide formation in methane oxidation to methanol, Science 367 (2020) 193–197, https://doi.org/10.1126/science.aaw1108.

[13] S. Bai, F. Liu, B. Huang, F. Li, H. Lin, T. Wu, M. Sun, J. Wu, Q. Shao, Y. Xu, X. Huang, High-efficiency direct methane conversion to oxygenates on a cerium dioxide nanowires supported rhodium single-atom catalyst, Nat. Commun. 11 (2020) 954, https://doi.org/10.1038/s41467-020-14742-x.

[14] Q. Shen, C. Cao, R. Huang, L. Zhu, X. Zhou, Q. Zhang, L. Gu, W. Song, Single chromium atoms supported on titanium dioxide nanoparticles for synergic catalytic methane conversion under mild conditions, Angew. Chem. Int. Ed. 59 (2020) 1216–1219, https://doi.org/10.1002/anie.201913309.

[15] T. Yu, Z. Li, W. Jones, Y. Liu, Q. He, W. Song, P. Du, B. Yang, H. An, D.M. Farmer, C. Qiu, A. Wang, B.M. Weckhuysen, A.M. Beale, W. Luo, Identifying key mononuclear Fe species for low-temperature methane oxidation, Chem. Sci. 12 (2021) 3152–3160, https://doi.org/10.1039/d0sc06067d.

[16] L. Luo, J. Luo, H. Li, F. Ren, Y. Zhang, A. Liu, W.-X. Li, J. Zeng, Water enables mild oxidation of methane to methanol on gold single-atom catalysts, Nat. Commun. 12 (2021) 1218, https://doi.org/10.1038/s41467-021-21482-z.

[17] S.J. Freakley, N. Dimitratos, D.J. Willock, S.H. Taylor, C.J. Kiely, G.J. Hutchings, Methane oxidation to methanol in water, Acc. Chem. Res. 54 (2021) 2614–2623, https://doi.org/10.1021/acs.accounts.1c00129.

[18] F. Gu, X. Qin, M. Li, Y. Xu, S. Hong, M. Ouyang, G. Giannakakis, S. Cao, M. Peng, J. Xie, M. Wang, D. Han, D. Xiao, X. Wang, Z. Wang, D. Ma, Selective catalytic oxidation of methane to methanol in aqueous medium over copper cations promoted by atomically dispersed rhodium on TiO_2, Angew. Chem. Int. Ed. 61 (2022), e202201540, https://doi.org/10.1002/anie.202201540.

[19] Y. Tang, Y. Li, F. Tao, Activation and catalytic transformation of methane under mild conditions, Chem. Soc. Rev. 51 (2022) 376–423, https://doi.org/10.1039/D1CS00783A.

[20] B. Wu, T. Lin, M. Huang, S. Li, J. Li, X. Yu, R. Yang, F. Sun, Z. Jiang, Y. Sun, L. Zhong, Tandem catalysis for selective oxidation of methane to oxygenates using oxygen over PdCu/zeolite, Angew. Chem. Int. Ed. 61 (2022), e202204116, https://doi.org/10.1002/anie.202204116.

[21] A. Oda, K. Aono, N. Murata, K. Murata, M. Yasumoto, N. Tsunoji, K. Sawabe, A. Satsuma, Rational design of ZSM-5 zeolite containing a high concentration of single Fe sites capable of catalyzing the partial oxidation of methane with high turnover frequency, Catal. Sci. Technol. 12 (2022) 542–550, https://doi.org/10.1039/D1CY01987B.

[22] K. Ohkubo, K. Hirose, Light-driven C–H oxygenation of methane into methanol and formic acid by molecular oxygen using a perfluorinated solvent, Angew. Chem. Int. Ed. 57 (2018) 2126–2129, https://doi.org/10.1002/anie.201710945.

[23] K. Zhu, S. Liang, X. Cui, R. Huang, N. Wan, L. Hua, H.Y. Li, H. Chen, Z. Zhao, G. Hou, M. Li, Q. Jiang, L. Yu, D. Deng, Highly efficient conversion of methane to formic acid under mild conditions at ZSM-5-confined Fe-sites, Nano Energy 82 (2021), 105718, https://doi.org/10.1016/j.nanoen.2020.105718.

[24] Y. Xing, Z. Yao, W. Li, W. Wu, X. Lu, J. Tian, Z. Li, H. Hu, M. Wu, Fe/Fe_3C boosts H_2O_2 utilization for methane conversion overwhelming O_2 generation, Angew. Chem. Int. Ed. 60 (2021) 8889–8895, https://doi.org/10.1002/anie.202016888.

[25] X. Yu, B. Wu, M. Huang, Z. Lu, J. Li, L. Zhong, Y. Sun, IrFe/ZSM-5 synergistic catalyst for selective oxidation of methane to formic acid, Energy Fuels 35 (2021) 4418–4427, https://doi.org/10.1021/acs.energyfuels.0c04198.

[26] R.A. Periana, O. Mironov, D. Taube, G. Bhalla, C.J. Jones, Catalytic, oxidative condensation of CH_4 to CH_3COOH in one step via CH activation, Science 301 (2003) 814–818, https://doi.org/10.1126/science.1086466.

[27] X. Wang, G. Qi, J. Xu, B. Li, C. Wang, F. Deng, NMR-spectroscopic evidence of intermediate-dependent pathways for acetic acid formation from methane and carbon monoxide over a ZnZSM-5 zeolite catalyst, Angew. Chem. Int. Ed. 51 (2012) 3850–3853, https://doi.org/10.1002/anie.201108634.

[28] J.-F. Wu, S.-M. Yu, W.D. Wang, Y.-X. Fan, S. Bai, C.-W. Zhang, Q. Gao, J. Huang, W. Wang, Mechanistic insight into the formation of acetic acid from the direct conversion of methane and carbon dioxide on zinc-modified H–ZSM-5 zeolite, J. Am. Chem. Soc. 135 (2013) 13567–13573, https://doi.org/10.1021/ja406978q.

[29] K. Narsimhan, V.K. Michaelis, G. Mathies, W.R. Gunther, R.G. Griffin, Y. Román-Leshkov, Methane to acetic acid over Cu-exchanged zeolites: Mechanistic insights from a site-specific carbonylation reaction, J. Am. Chem. Soc. 137 (2015) 1825–1832, https://doi.org/10.1021/ja5106927.

[30] J. Shan, M. Li, L.F. Allard, S. Lee, M. Flytzani-Stephanopoulos, Mild oxidation of methane to methanol or acetic acid on supported isolated rhodium catalysts, Nature 551 (2017) 605–608, https://doi.org/10.1038/nature24640.

[31] Y. Tang, Y. Li, V. Fung, D. Jiang, W. Huang, S. Zhang, Y. Iwasawa, T. Sakata, L. Nguyen, X. Zhang, A.I. Frenkel, F. Tao, Single rhodium atoms anchored in micropores for efficient transformation of methane under mild conditions, Nat. Commun. 9 (2018) 1231, https://doi.org/10.1038/s41467-018-03235-7.

[32] Y. Sun, The investigation of the Fe-modified ZSM-5 zeolite catalyzing the formation of acetic acid from methane and carbon monoxide, Lanzhou University, 2021.

[33] B. Li, X. Song, S. Feng, Q. Yuan, M. Jiang, L. Yan, Y. Ding, Direct conversion of methane to oxygenates on porous organic polymers supported Rh mononuclear complex catalyst under mild conditions, Appl. Catal. B 293 (2021), 120208, https://doi.org/10.1016/j.apcatb.2021.120208.

[34] B. Wu, T. Lin, Z. Lu, X. Yu, M. Huang, R. Yang, C. Wang, C. Tian, J. Li, Y. Sun, L. Zhong, Fe binuclear sites convert methane to acetic acid with ultrahigh selectivity, Chem. 8 (2022) 1658–1672, https://doi.org/10.1016/j.chempr.2022.02.001.

[35] T. Moteki, N. Tominaga, M. Ogura, Mechanism investigation and product selectivity control on CO-assisted direct conversion of methane into C1 and C2 oxygenates catalyzed by zeolite-supported Rh, Appl. Catal. B 300 (2022), 120742, https://doi.org/10.1016/j.apcatb.2021.120742.

[36] G. Qi, T.E. Davies, A. Nasrallah, M.A. Sainna, A.G.R. Howe, R.J. Lewis, M. Quesne, C.R.A. Catlow, D.J. Willock, Q. He, D. Bethell, M.J. Howard, B.A. Murrer, B. Harrison, C.J. Kiely, X. Zhao, F. Deng, J. Xu, G.J. Hutchings, Au-ZSM-5 catalyses the selective oxidation of CH_4 to CH_3OH and CH_3COOH using O_2, Nat. Catal. 5 (2022) 45–54, https://doi.org/10.1038/s41929-021-00725-8.

[37] C. Tu, X. Nie, J.G. Chen, Insight into acetic acid synthesis from the reaction of CH_4 and CO_2, ACS Catal. 11 (2021) 3384–3401, https://doi.org/10.1021/acscatal.0c05492.

[38] P.M. Maitlis, A. Haynes, G.J. Sunley, M.J. Howard, Methanol carbonylation revisited: Thirty years on, J. Chem. Soc., Dalton Trans. (1996) 2187–2196, https://doi.org/10.1039/DT9960002187.

[39] M.V. Luzgin, V.A. Rogov, N.S. Kotsarenko, V.P. Shmachkova, A.G. Stepanov, Methane carbonylation with CO on sulfated zirconia: Evidence from solid-state NMR for the selective formation of acetic acid, J. Phys. Chem. C 111 (2007) 10624–10629, https://doi.org/10.1021/jp0728757.

[40] T. Moteki, N. Tominaga, M. Ogura, CO-assisted direct methane conversion into C_1 and C_2 oxygenates over ZSM-5 supported transition and platinum group metal catalysts using oxygen as an oxidant, ChemCatChem 12 (2020) 2957–2961, https://doi.org/10.1002/cctc.202000168.

[41] M.S. Kumar, M. Schwidder, W. Grünert, A. Brückner, On the nature of different iron sites and their catalytic role in Fe-ZSM-5 $DeNO_x$ catalysts: New insights by a combined EPR and UV/VIS spectroscopic approach, J. Catal. 227 (2004) 384–397, https://doi.org/10.1016/j.jcat.2004.08.003.

[42] M.S. Kumar, M. Schwidder, W. Grünert, U. Bentrup, A. Brückner, Selective reduction of NO with Fe-ZSM-5 catalysts of low Fe content: Part II. Assessing the function of different Fe sites by spectroscopic in situ studies, J. Catal. 239 (2006) 173–186, https://doi.org/10.1016/j.jcat.2006.01.024.

[43] T. Yamashita, P. Hayes, Analysis of XPS spectra of Fe^{2+} and Fe^{3+} ions in oxide materials, Appl. Surf. Sci. 254 (2008) 2441–2449, https://doi.org/10.1016/j.apsusc.2007.09.063.

[44] S. Shwan, R. Nedyalkova, J. Jansson, J. Korsgren, L. Olsson, M. Skoglundh, Hydrothermal stability of Fe–BEA as an NH_3-SCR catalyst, Ind. Eng. Chem. Res. 51 (2012) 12762–12772, https://doi.org/10.1021/ie301516z.

[45] W.-H. Feng, M.-M. Yu, L.-J. Wang, Y.-T. Miao, M. Shakouri, J. Ran, Y. Hu, Z. Li, R. Huang, Y.-L. Lu, D. Gao, J.-F. Wu, Insights into bimetallic oxide synergy during carbon dioxide hydrogenation to methanol and dimethyl ether over $GaZrO_x$ oxide catalysts, ACS Catal. 11 (2021) 4704–4711, https://doi.org/10.1021/acscatal.0c05410.

[46] J. Zhang, Y.Y. Chu, F. Deng, Z. Feng, X. Meng, F.-S. Xiao, Evolution of D6R units in the interzeolite transformation from FAU, MFI or *BEA into AEI: Transfer or reassembly, Inorg. Chem. Front. 7 (2020) 2204–2211, https://doi.org/10.1039/D0QI00359J.

[47] A.M. Mofrad, C. Peixoto, J. Blumeyer, J. Liu, H.K. Hunt, K.D. Hammond, Vibrational spectroscopy of sodalite: Theory and experiments, J. Phys. Chem. C 122 (2018) 24765–24779, https://doi.org/10.1021/acs.jpcc.8b07633.

[48] J.F. Wu, W.D. Wang, J. Xu, F. Deng, W. Wang, Reactivity of C_1 surface species formed in methane activation on Zn-modified H-ZSM-5 zeolite, Chem. – Eur. J. 16 (2010) 14016–14025, https://doi.org/10.1002/chem.201002258.

[49] The 0.5% Fe/ZSM-5 catalyst was prepared by solid state ion-exchange method. J. Li, M.-M. Yu, Y. Sun, W.-H. Feng, Z. Feng, J.-F. Wu, Effect of aqueous solution pH on the oxidation of methane to methanol at low temperature Chem. J. Chin. Univ. 42 (2021) 776–783, https://doi.org/10.7503/cjcu20200703.

[50] T. Kinnunen, K. Laasonen, The oxidative addition and migratory 1,1-insertion in the Monsanto and Cativa processes. A density functional study of the catalytic carbonylation of methanol, J. Mol. Struct.: THEOCHEM 542 (2001) 273–288, https://doi.org/10.1016/S0166-1280(00)00859-9.

[51] A.W. Budiman, J.S. Nam, J.H. Park, R.I. Mukti, T.S. Chang, J.W. Bae, M.J. Choi, Review of acetic acid synthesis from various feedstocks through different catalytic processes, Catal. Surv. Asia 20 (2016) 173–193, https://doi.org/10.1007/s10563-016-9215-9.

[52] M.H. Ab Rahim, M.M. Forde, R.L. Jenkins, C. Hammond, Q. He, N. Dimitratos, J. A. Lopez-Sanchez, A.F. Carley, S.H. Taylor, D.J. Willock, D.M. Murphy, C.J. Kiely, G.J. Hutchings, Oxidation of methane to methanol with hydrogen peroxide using supported gold–palladium alloy nanoparticles, Angew. Chem. Int. Ed. 52 (2013) 1280–1284, https://doi.org/10.1002/anie.201207717.

[53] H. Song, X. Meng, S. Wang, W. Zhou, X. Wang, T. Kako, J. Ye, Direct and selective photocatalytic oxidation of CH_4 to oxygenates with O_2 on cocatalysts/ZnO at room temperature in water, J. Am. Chem. Soc. 141 (2019) 20507–20515, https://doi.org/10.1021/jacs.9b11440.

[54] G.-Q. Xu, T.-F. Xiao, G.-X. Feng, C. Liu, B. Zhang, P.-F. Xu, Metal-free α-C(sp^3)–H aroylation of amines via a photoredox catalytic radical-radical cross-coupling process, Org. Lett. 23 (2021) 2846–2852, https://doi.org/10.1021/acs.orglett.1c00226.

[55] E. Stavitski, B.M. Weckhuysen, Infrared and Raman imaging of heterogeneous catalysts, Chem. Soc. Rev. 39 (2010) 4615–4625, https://doi.org/10.1039/C0CS00064G.
[56] S. Jin, Z. Feng, F. Fan, C. Li, UV Raman spectroscopic characterization of catalysts and catalytic active sites, Catal. Lett. 145 (2015) 468–481, https://doi.org/10.1007/s10562-014-1416-0.
[57] C. Hess, New advances in using Raman spectroscopy for the characterization of catalysts and catalytic reactions, Chem. Soc. Rev. 50 (2021) 3519–3564, https://doi.org/10.1039/D0CS01059F.
[58] H. Xia, K. Sun, Z. Liu, Z. Feng, P. Ying, C. Li, The promotional effect of NO on N_2O decomposition over the bi-nuclear Fe sites in Fe/ZSM-5, J. Catal. 270 (2010) 103–109, https://doi.org/10.1016/j.jcat.2009.12.014.
[59] C. Hammond, I. Hermans, N. Dimitratos, Biomimetic oxidation with Fe-ZSM-5 and H_2O_2? Identification of an active, extra-framework binuclear core and an Fe^{III}–OOH intermediate with resonance-enhanced raman spectroscopy, ChemCatChem 7 (2015) 434–440, https://doi.org/10.1002/cctc.201402642.
[60] S. Kameoka, T. Nobukawa, S. Tanaka, S. Ito, K. Tomishige, K. Kunimori, Reaction between N_2O and CH_4 over Fe ion-exchanged BEA zeolite catalyst: A possible role of nascent oxygen transients from N_2O, Phys. Chem. Chem. Phys. 5 (2003) 3328–3333, https://doi.org/10.1039/B300562N.
[61] T. Yu, Y. Su, A. Wang, B.M. Weckhuysen, W. Luo, Efficient synthesis of monomeric Fe species in zeolite ZSM-5 for the low-temperature oxidation of methane, ChemCatChem 13 (2021) 2766–2770, https://doi.org/10.1002/cctc.202100299.